Failure mechanisms and triggering factors in calcareous cliffs of the Subalpine ranges (French Alps)

Magali Frayssines, Didier Hantz

Failure mechanisms and triggering factors in calcareous cliffs of the Subalpine ranges (French Alps)

M. Frayssines*, D. Hantz

Université Joseph Fourier, Grenoble, France

*Corresponding author. Magali.Frayssines@ujf-grenoble.fr
Fax: +33 476 82 80 70

Abstract
In order to enhance the detection of prospective rock falls in calcareous cliffs, 25 rock falls have been described in a more detailed way than for an inventory. They are representative of middle size rock falls (10 to 100,000 m^3) occurring in the French Subalpine Ranges, at an elevation between 200 m and 2,000 m. Structural conditions of the rock masses, morphology of the initial cliff surface and the scar, possible failure mechanisms and processes have been studied. Typical failure configurations have been identified, based on the attitude of the failure surface, in relation to the bedding planes and the cliff surface. Irregular cliff morphology appears to be another important susceptibility factor. In most cases, the classical comparison of the average planes of the main joint sets with the average plane of the slope could not define the potentially unstable masses. Rather, those ones are due to joint planes that deviate from their mean set plane or to irregularities of the cliff surface. The proposed investigation method to detect prospective rock falls mainly consists in observing stereoscopic aerial photographs in order to look for critical configurations. Once a critical mass has been detected, its failure probability for a period of the order of one century must be evaluated (or its life expectancy). The main factor to consider for this purpose appears to be the proportion of rock bridges in the potential failure surface.
The triggering factors of rock falls in our study area have been investigated, by analysing an inventory of 46 rock falls. Statistical tests have been carried out to study the relation between rock falls and daily rainfall, freeze-thaw cycles or earthquakes. A good correlation has been obtained with freeze-thaw cycles, a slight correlation with rainfall and no correlation with earthquakes. This suggests that ice jacking could the main physical process leading to failure by causing microcrack propagation.

1. Introduction

Varnes (1984) proposed a widely adopted definition for landslide hazard as "the probability of occurrence of a potentially damaging phenomenon (landslide) within a given area and in a given period of time". In the case of rock falls and rock avalanches, the damaging phenomenon results from the failure of a rock mass and its propagation down to the given area. It ensues that the rock fall hazard equals the failure probability multiplied by the probability of propagation. Different probabilistic methods exist to calculate the probability of propagation (for example, Guzzetti et al., 2002; Labiouse, 2004; Jaboyedoff et al., 2005). Probabilistic

geomechanical analyses make it possible to calculate the failure probability, i.e. the probability that a designed future slope will fail when it will be cut (for example, Scavia et al., 1990). These models permit not to calculate the probability that an existing stable slope will fail in a given time period. A failure prediction is only possible for accelerating rockslides, by analysing the monitored displacements (Federico et al., 2004).

At the present time, failure hazard evaluation for land use planning can be based on 1) expert judgement, 2) on empirical rating methods (Jaboyedoff et al., 1999; Mazzocola and Sciesa, 2000; Dussauge-Peisser, 2002) or 3) on rock fall inventories (Chau et al., 2003; Coe et al., 2005). Approach 1) gives a qualitative and subjective evaluation of failure hazard. Approach 2) doesn't evaluate the failure probability, but the susceptibility to rock falls. The susceptibility does not take the temporal component of the hazard into account in a quantitative way. Note that the statistical approach developed for landslides (Aleotti and Chowdhury, 1999) is rarely applied to rock falls, due to the lack of rock fall specific databases. The temporal component of failure hazard can be approached with rock fall inventories (historical approach, approach 3). They make it possible to estimate rock fall frequencies in areas that have to be considered as homogeneous (for example, Evans and Hungr, 1993; Wieczorek et al., 1999; Dussauge-Peisser et al., 2002; Chau et al., 2003; Wieczorek and Snyder, 2004). Knowing the temporal distribution of rock falls of a given volume range, the probability that n failures occur in a given area can be calculated (Hantz et al., 2003). But the places where the failures can occur and the individual failure probability of each potentially unstable rock mass are not given by the historical approach.

The main objective of the study presented in this paper is to enhance the detection of potentially unstable rock masses in calcareous cliffs, thanks to a better knowledge of the intrinsic conditions and causal processes of the rock falls, according to the principle that slope failures in the future will be more likely to occur under the conditions which led to past instability (Guzzetti et al., 1999). For this purpose, a first database has been constructed, in which 25 rock falls have been described in a more detailed way than for a basic inventory. Structural conditions of the rock masses, morphology of the initial cliff and the scar, possible failure mechanisms and processes have been studied. A second database, including 46 rock falls, has been elaborated to analyse the relation between rock falls and climatic and seismic factors.

2. Geological, geomorphological and seismic context

2.1. Geology

Our study area is located in the sedimentary cover of the External Crystalline Massifs of the French Western Alps (Belledonne, Mont Blanc, etc.) which belong to the Dauphinoise (or Helvetic) zone (figure 1). These massifs underwent crustal shortening in the direction E-W to NW-SE, which began 20-30 Ma ago, and presently undergo an uplift at a rate of the order of 1 mm/year. This shortening also deformed and transported towards the NW a part of the Mesozoic cover, which now forms the Northern Subalpine Ranges (Vercors, Chartreuse, Bauges, etc.). The main resulting structural features are thrust faults and folds inclined westwards. These ranges are made of limestone and marls from the upper Jurassic and Cretaceous age. Typically, valley walls consist of a succession of steep calcareous cliffs and marly slopes, between 200 m and 2,000 m in elevation. The calcareous

cliffs belong to Tithonian, Valanginian, Barremian (Urgonian facies), and Campanian-Maastrichtian (Senonian) stages. The more prominent cliffs in the landscape are the Tithonian and Urgonian ones. The highest cliffs are up to 450 m high. Typically, the limestone beds are cut perpendicularly by 2 joint sets. They have been affected by karst dissolution, which have enlarged some joints.

2.2. Climate
At the Saint Martin d'Hères station (212 m), which is located near Grenoble between the Chartreuse and Vercors massifs (figures 1 and 13), a continental climate prevails. The mean annual temperature is 11.4°C and the mean annual rainfall is 992 mm. The monthly rainfall and temperature, for the 1971-2000 period, are given in figure 2. The climate is marked by hot summers (average August temperature of 28°C) and harsh winters (average January temperature of -1°C). Rainfalls are quite sustained along the year, but July and August correspond to a relative dry period. The maximal daily rainfall since 1946 is 135.5 mm. In the Chartreuse and Vercors massives, a mountain climate prevails, where temperatures and precipitations are mainly influenced by the elevation. For example, at the Autrans station (1,060 m) located in the Vercors massif (figure 1), the mean annual temperature is 6.1°C and the mean annual rainfall is 1,459 mm. During the 1984-1985 cold season, freeze period (without thaw) represents 47% of the total period at 2500 m, 11% at 1,350 m and 5% at 800 m (Rovera, 1990). The studied rock falls are located between the elevations of 200 and 2,000 m.

2.3. Seismicity
According to the seismic hazard map of the European-Mediterranean region (Jimenez et al., 2001), the 475-year return period peak ground acceleration in our study area is about 1.5 m/s^2 (in other words, the probability for this value to be exceeded in a 50-year period is 10%). In the Helvetic zone around Grenoble, no clear seismicity pattern can be recognized, except the recently discovered Subalpine seismic arc, which corresponds more or less to the Belledone Middle Fault in the area shown in the figure 1. In the 1989-2002 period, 150 earthquakes have occurred along this arc at a depth of 5 to 10 km, with as great as M3.5 (Thouvenot and Fréchet, 2004).

2.4. Rock fall frequency
A rock fall inventory for the Grenoble area has been made by a forest service (RTM), which have recorded rock falls occurring before and during the 20th century, which have left physical or historical traces (Hantz et al., 2003). Using a power law distribution of the rock fall volumes, the mean failure frequencies for the investigated 150 km of cliff located in the study area have been estimated as 65, 18 and 5 events per century for the volume ranges of 10^2-10^3, 10^3-10^4, and 10^4-10^5 m^3. In 1248, a huge rock slide (at least 200 10^6 m^3) affected the north wall of the Mount Granier, in the Chartreuse Massif (Goguel and Pachoud, 1972 ; Antoine and Cruden, 1984). The sliding surface took place in the Valanginian marls underlying the Hauterivian and Urgonian strata. Because the main failure mechanism did not take place in the calcareous cliff, this rock slide was not considered in the inventory or in the present study.

3. The databases

Two databases of occurred rock falls have been elaborated for two different purposes. The first database (1) is aimed to study the intrinsic ground conditions that can favour rock falls, and the failure mechanisms of middle size (25-50,000 m³) rock falls occurring in the calcareous cliffs. The objective of the second database (2) is to identify the triggering factors of rock falls and then to better understand their failure processes. Contrary to the RTM inventory, these databases are not supposed to be exhaustive. They are supposed to be representative samples of the rock falls occurring in the Subalpine Ranges. Most of them took place in the Vercors and Chartreuse Massifs. One rock fall occurred in the sedimentary border hills of Belledonne massif, made of marl and marly limestone of Lias to Dogger stages.

3.1. Database (1)

Database (1) contains geometrical, structural and mechanical information concerning 25 rock falls whose location is shown in figure 13. The data are shown in tables 1 and 2. The rock falls have been found from either the RTM inventory (for the older ones), the media (local radios and newspapers), or from continuous observation of the cliffs in the Grenoble area. Most of them have a volume greater than 100 m³ and have been easily identified thanks to the bright scar they left (in contrast with the patina of the cliff), and the damage they produced in the forest (figure 3). The scars have been surveyed, sometimes using rope, in order to collect geometrical and structural information: dimensions, intact rock fracture, discontinuities making up the failure surface (orientation, extension, roughness, cover).

3.2. Database (2)

Database (2) contains 46 rock falls that occurred between 1970 and 2004, whose day of occurrence is known. Their volume varies from 10 m³ to 30,000 m³. Most of them belong to the RTM inventory, the other being posterior to the inventory, and 12 belong also to database (1). They all occur in the same area than rock falls of database (1).

4. Description of the scars, initial slopes and possible failure mechanisms (database 1)

4.1. Chronological, geological and geometric data

Chronological, geological and morphometric data of the investigated rock falls are given in table 1. The day of occurrence is known for 12 rock falls, which caused damages or propagated close to buildings. The other rock falls propagated in forested areas and reached a path in some cases. Most of the failures (17) occurred in Urgonian limestone. The attitude of the beds with regard to the cliff is described by four configurations: horizontal (dip < 10°), transverse (the angle α between the cliff direction and the bedding strike is greater than 45°), conform ($\alpha < 45°$ and dip towards the valley), inverse ($\alpha < 45°$ and dip towards the mountain). The maximal length and width of the scar were precised in accordance with the IAEG (1990), but it is necessary to precise that the scar length may include a possible opening surface. The area of the scar was estimated from photographs and in situ measurement of the scar. The term thickness was preferred to depth, used for

landslides by the IAEG. The thickness is measured normally to the main scar surface and refers to the initial cliff surface. In most cases, it was roughly estimated from photographs of the initial state (when available) or by interpolating the cliff morphology on both sides of the scar. It ensues that the initial volume is also roughly estimated. These data will be used to characterise the geometric conditions of rock falls.

4.2. Typical failure configurations

Before describing the typical configurations that have led to rock falls, it is necessary to define some important terms that will be used. In accordance with the landslide classifications proposed by the IAEG (1990) and Cruden and Varnes (1996), the first movement preceding the rock fall can be a slide or a topple. According to Hutchinson (1988), slides can be divided into rotational slides, translational slides and compound slides. Furthermore, translational slides can occur on one plane (planar slide), on two (non parallel) planes (wedge slide), on one joint set (stepped slide) or on two joint sets (stepped wedge slide). Compound slides are characterised by slip surfaces formed of a combination of a steep rearward part and a flatter sole. They imply the development of internal displacements and shears. The surfaces forming the scar will be divided in three types: sliding surfaces, pure shear surfaces and opening surfaces. Pure shear surfaces are shear surfaces, which don't undergo a normal stress. Therefore, they exert a resisting force only if they have cohesion. Theoretically, a pure shear plane must intersect a sliding plane exactly along its dip. It is a limit case between a sliding plane and an opening plane. In practice, lateral planes whose classification as sliding or opening is uncertain will be called (pure) shear planes. Opening of a joint can be caused by a slide or a topple.

In some cases, it is not possible to know if an overhanging slab or a column has slid or toppled. For this reason, the observed cases will be classified according to their geometric configuration, rather than their failure mechanism (figure 4). The proposed practical classification can be used for the detection of potential rock falls, for which the same uncertainty exists.

A. Bedding conform to the slope (3 cases)

The overall slope surface is roughly parallel to the bedding, but bedding joints daylight in a place where the slope surface is locally steeper than bedding (figure 4A). This may be due to natural or manmade undercutting. We have no case, where the overall slope surface is clearly steeper than bedding. In configuration A, the type of movement is a translational slide, described as bed slide in table 2.

B. Bedding dipping less than 30° opposite to the slope (19 cases)

In this situation, the slope forms a steep cliff. In most cases, the cliff strikes nearly parallel to one main joint set. A rock fall may occur in two different configurations.

B1. Some joints define a potential translational sliding surface, roughly planar or wedge-shaped (figure 4B1). They usually belong to the main joint set (perpendicular to the bedding). Frequently, the potential failure surface daylights in an overhang, due to either a weaker layer or a precedent failure.

B2. The main joints (perpendicular to the bedding) don't daylight and another (smaller) failure surface is necessary to cut a removable block (figure 4B2). This surface is less steep than the main joints, and is made of pre-existing or new cracks (i.e. due to intact rock fracturing). It may be a basal sliding surface or an opening surface, in case of toppling. In case of sliding, the mechanism may be a

translational slide on the small failure surface, with opening of the main joints, or a compound slide.

If the cliff surface presents a prominent overhang, the failure mechanism can be a topple, due to tensile fracturing of intact rock (in B1 or B2 configuration). A detailed digital model is necessary to determine if topple was possible. For some of the observed rock falls, the failure mechanism may be slide or topple. The most probable mechanism (given in table 2) has been determined qualitatively, from photographs of the initial stage (when available) or by interpolating the cliff morphology on both sides of the scar.

C. Bedding dipping more than 30° opposite to the slope (3 cases)

Joints belonging to the main joint set (perpendicular to the bedding)

define a potential translational sliding surface, which is usually strongly stepped, with bedding planes forming overhangs (figure 4C).

In any configuration (A, B or C), the moving mass must be removable in 3 dimensions. In some cases, it needs to be cut laterally by joints or free surfaces. Joints may act as secondary sliding plane, shear plane or opening plane. The nature and position (right or left) of the lateral surfaces are given in table 2. Furthermore, table 2 indicates if the scar is limited rearwards by an opening surface or not. The position of the scars on the cliff is indicated in figure 5. The form of the scars is characterised by the fact that, in most cases (21 from 25), the width of the scar is less than the length (figure 6A).

4.3. Surface of the scars

An important point for the mechanical analysis of rock falls is the existence of intact rock fracturing, which has been observed on some scars. This point has already been noted by many authors (Terzaghi, 1962; Robertson, 1970; Einstein et al., 1983; Eberhardt et al., 2004). Intact rock fracturing is indicated by the colour of fresh intact rock, which is light beige to light rosy for Urgonian limestone and dark grey for Thitonian limestone. Fresh fracture surfaces usually contrast with the rest of the scar, which is often coated with a calcite crust (figure 7), whose colour may vary from white to orange, according to the quantity of iron oxide in the calcite. These surfaces usually represent a very small part of the scar area (table 2) and their observation needs roping down in the cliff. They may result from fracturing of rock bridges or bumps on sliding planes. Bumps fracturing may be caused by the friction of the moving mass after the initial failure. Intact rock fracturing can occur on translational sliding surfaces (shear mode), on rear opening surfaces (tensile mode) or on small basal surfaces (B2 configuration), which can be sliding surfaces or opening surfaces in case of toppling. The proportion of intact rock fracture on the scar and the fracture mode are given in the table 2.

Intact rock fractures have been observed on all of the translational sliding surfaces dipping more than 50°, which have been closely observed by roping down. Intact rock fracturing permits to explain that such potentially unstable masses had been stable probably for several centuries. They were retained by rock bridges (or prominent bumps), that give cohesion to the sliding planes and whose failure triggered the fall of the mass. Assuming that the rock bridges have the same cohesion, the cohesion of a sliding plane is proportional to the percentage of rock bridges in this plane. One can expect that the cohesion required to ensure limit equilibrium of a rock mass depends on its thickness. For a parallelepipedal block resting on an inclined plane, it can be easily demonstrated that this cohesion is proportional to the thickness of the block. Thus, one can expect that the percentage

of rock bridges on the scars is roughly proportional to the thickness of the fallen masses. As can be seen on figure 8, our observations are consistent with this theoretical result. One intact rock fracture has been observed on the rear opening surface of a planar slide dipping at 50°. A rock bridge gave the necessary tensile strength to resist to sliding. In the case of potential toppling, rock bridges also gave the necessary tensile strength to explain the passed stability. The mechanical parameters which determine the stability of a rock mass are the friction angles of the joints and the rock bridges, and the cohesion and tensile strength of the rock bridges. Due to the huge uncertainty on the proportion of rock bridges in potential failure surfaces, the uncertainty is far larger on the cohesion and tensile strength than on the friction angles. Thus, the persistence of the joints appears to be the main factor to consider in the evaluation of the failure probability.

An important question for the detection of future rock falls is to know if the main parts of the potential scars are open or not before the failure. If they are sufficiently open, they could be detected by geophysical prospecting (Dussauge-Peisser et al., 2003). Most of the scars which have been closely observed are covered with a hard calcite crust, calcite crystals or karst concretion (figure 7). Near the top surface of the cliff, tufa has also been observed. This indicates that these scars have been open for a long time and water has seeped inside. Other failure surfaces (or parts of them) have used small closed cracks, filled with calcite, rather than joints belonging to main joint sets which can be identified on the cliff before the fall. In these cases, the failure surface is very irregular.

4.4. Initial morphology of the cliff

We have attempted to describe the initial morphology of the fallen mass in order to detect morphological features that are prone to rock falls. Vertical and horizontal sections of the initial cliff have been considered in table 2 and in figure 9. In both sections, the fallen mass could be prominent or not. If it was prominent in horizontal section, it could have formed a step, a spur or a tower. In the vertical section, it could have formed a roof, an inclined step, a slightly overhanging surface (slope angle just exceeding 90°), or comprise a local overhang at the toe of the scar.

5. Triggering factors and failure processes (database 2)

5.1. Climatic factors

Figure 10 shows the annual distribution of the rock falls. It appears that rock falls are more frequent during December, January and February. Moreover, the 7 biggest rock falls mentioned in table 1 occurred from January to April. Contrary to rock falls, monthly rainfalls are the most important in September, October and November (figure 2). The potential influence of daily rainfall has been also studied by comparing the distribution of all the daily rainfalls in the 1970-2004 period (12,389 days), by determining which and how much daily rainfall occurred the same day as the rock falls (46 days), in the same period (figure 11). The mean value of the second distribution (3.8 mm) is higher than the one of the first distribution (2.7 mm). At first sight, this suggests that daily rainfall influences rock falls. But the Kolmogorov-Smirnov test (Cheeney, 1983) shows that this difference is not significant, according to the small size of the second population (46 days with a rock fall) compared to the size of the first one (12,389 days without rock fall): The maximum discrepancy D between the two cumulative distribution functions is 0.163; this value has a probability greater than 0.05 to be reached, should both

populations be identical. Thus, the hypothesis of a null influence of rainfall can not be rejected. The same conclusion is reached when considering 2-day cumulative rainfalls.

Our data don't prove the influence of rainfall on rock falls, contrary to the results of Chau et al. (2003) concerning rock falls in Hong Kong, where a good correlation was found between daily rainfall and rock falls. But there are two important differences between the two data sets: first, the rock fall volumes in the Hong Kong data are smaller than those in Grenoble (50% are less than 1 m^3 in Hong Kong, they are all greater than 10 m^3 in Grenoble); second, the daily rainfall in Hong Kong can exceed 300 mm, whereas it does not reach 100 mm at the Saint-Martin d'Hères station (212 m) and is probably less than 200 mm at the higher rock fall scars.

As said before, rock falls are more frequent in December, January and February (figure 10). These months are the coldest ones in the year, but the mean daily maximal temperature is still positive in most of the failure sites. This means that variations of temperature around the freezing point are frequent in this period. The influence of these variations has been analysed from the contingency table 3A. The first column shows the number of days with a rock fall and a freeze-thaw cycle, against the number with a rock fall and without freeze and thaw. The second column shows the number of days without rock fall and with freeze and thaw, against the number without rock fall and freeze and thaw. A chi-squared test (Cheeney, 1983) has been performed to test the independence between rock falls and freeze and thaw. The obtained χ^2 value, which expresses the deviation from the hypothesis of independence, is 9.85. The probability to obtain such a high value, should the factors be independent, is less than 0.01. Our data show a significant correlation between rock falls and freeze-thaw cycles. Note that a good correlation (deviation equal to 9.33) is also obtained when considering freeze (not necessarily freeze and thaw). Our conclusion is in agreement with the result of a statistical analysis of rock falls in Norway (Sandersen et al., 1996). The distribution of rock falls along the year shows two maxima, in early spring and late autumn, which coincides, in Norway, with the periods of frequent variations of temperature around the freezing point. The first maximum also coincides with the time of highest rate of snowmelt, the other with the months of highest precipitation. Our distribution shows a secondary maximum in April, which is the month when snowmelt is the most intense between 1,000 and 2,000 m elevations. An analysis of the rock fall activity in the Hosozawa Cirque, Japon (Matsuoka and Sakai, 1999), concluded that the intense activity does not reflect precipitation events. Nevertheless, the activity reaches its maximum in May-June, i.e. 5-15 days after the melt out of the cirque wall. A thermal conduction model suggests that a lag of 5-15 days would represent thaw penetration to a depth of about 1 m. The authors concluded that the primary factor controlling rock falls is seasonal frost weathering. Note that, contrary to our study area, Hosozawa Cirque underwent a deep frost penetration in winter.

5.2. Earthquakes

Figure 12 represents the peak ground accelerations greater than 10^{-4} ms^{-2}, measured near Grenoble, on the bedrock, from 1995 to 2004, by the French Accelerometric Network (Hatzfeld et al., 2003). The 12 rock falls which occurred in this period are represented by crosses and the number of days since the last earthquake is indicated for each rock fall, with the maximal horizontal acceleration of this earthquake. Only one rock fall occurred the same day than an earthquake, several hours later. This

earthquake produced a low acceleration of 4.6 10^{-4} ms^{-2}, but it is a replica of the strongest earthquake monitored in the observation period, which occurred two days before with an acceleration of 3.1 10^{-2} ms^{-2}. A statistical analysis of the contingency table 3B shows that the hypothesis of a null-(short-term) influence of earthquakes is very probable. Indeed the χ^2 value, which expresses the deviation from the hypothesis of independence, is only 0.07 and the probability to exceed this value, should the factors be independent, is about 0.8.

5.3. Failure processes

The analysis of the triggering factors allows proposing some possible failure processes for the observed rock falls. The good correlation between rock falls and frost suggests that ice jacking is the main failure process for the investigated volume range. Although the limestone in our study area is not very sensitive to freezing, ice jacking probably occurs in microcracks, which have formed near the limits of rock bridges. If the area of a rock bridge is critical, then ice jacking triggers failure. Otherwise, it induces microcrack propagation and rock weakening. Matsuoka and Sakai (1999) calculated the nocturnal and seasonal frost penetration due to heat conduction in a continuous rock mass and applied their result to the Hosozawa Cirque wall, which is made of sandstone and shale. In our study area, cliffs are made of limestone, in which joints have been enlarged by dissolution, permitting heat transfer by air flow in the open joints. It ensues that frost can penetrate more rapidly and deeper than in a relatively continuous rock mass. This suggests that nocturnal frost can produce rock falls, whose thickness reaches up to 10 m (figure 6B). Ice jacking needs frost and water. The morphological conditions in our study area are favourable to water seepage during thawing periods, because the plateau on the top of the cliffs is sufficiently flat to make snow accumulation possible.

Although the correlation between rock falls and rainfall appears very weak, the influence of water is suggested by the occurrence of numerous rock falls in April, when snowmelt is intense. Moreover, the good correlation between rock falls and freeze-thaw cycles may show not only the influence of freeze, but also the influence of thaw. Water seeping in the rock mass, while the outlet of natural drains is blocked up by ice, can be a triggering factor. A decrease of the rock strength due to increasing water content (Frayssines, 2005 ; Serratrice and Durville, 1997) can cause the failure if the stability of the rock mass is critical. In the climatic and seismic context of our study area, and during the observation period (1970-2004), freeze and water seepage, appear to be more active triggering factors than earthquakes. But, if no significant short term influence have been shown, earthquakes could weaken the rock mass and make it more susceptible to rock falls from other triggers (Keefer, 1984).

6. Detection of potential rock falls

Methods to detect potential failures in the framework of slope design are described, for example, in Hoek and Bray (1981). They are based on the comparison between the geological structure of the rock mass and the geometry of the slope, the geological structure being characterised by the average orientations of the different joint sets. In the block theory formulated by Goodman and Shi (1985), the joint pyramids are confronted with the excavation pyramid to detect the removable blocks. These methods are usually used to evaluate the stability of manmade cuts or

open pits, whose geometry must be determined according to economical or practical constraints (for example, the slope angle must be maximal or the cut direction is imposed by a transportation route). The role of geotechnical engineer is to minimize the probability that a failure occurs when the slope will be cut. How have the natural cliffs been "designed"? Figure 13 shows the mean cliff planes and the mean joint planes that have been determined from classical surveys of the cliffs, in the vicinity of the scars but without considering the failure surfaces. If bedding planes dip towards the valley (configuration A in figure 4), the slope surface is roughly parallel to bedding. If the bedding planes dip less than 30° in an inverse or transverse attitude (configuration B), the mean cliff plane is roughly parallel to a mean joint set (6 cases on the figure 13) or the intersection of two mean joint sets (2 cases). If the bedding planes dip more than 30° inwards the cliff (configuration C), the cliff surface is stepped, formed of bedding planes (forming overhangs) and one joint set dipping outwards the cliff. This suggests that erosion has used the potential sliding or opening planes to form the present calcareous cliffs of the Subalpine Ranges. In other words, most of the present slopes are made of scars of old rock falls.

In the context of hazard assessment at the scale of a valley wall, it ensues that in A and B configurations, the potentially unstable masses can not be detected by comparing the mean cliff plane and the mean joint planes, as usually done in slope design. Using the formulation of block theory (Goodman and Shi, 1985), the joint pyramids have at least a common limit with the excavation pyramid. So the joint pyramids don't define removable blocks. The potentially unstable masses must then be detected by looking for "deviations" from the mean cliff plane and the mean joint planes: morphological defaults of the cliff (figure 9, b to d and f to i), joint planes wandering from the mean orientation of their set (figure 4B1), or isolated joints (figure 4B2). This explains that the fallen rock masses are very thin in A and B configurations, as it can be seen in the figure 6B. In other words, the detection of failure configurations must be made at a local scale.

In the C configuration, the comparison between the mean cliff plane and the mean joint planes, shows that large rock masses are potentially unstable with the common hypothesis of infinite joints. But our observations show that cross joint extension is not large enough to allow the sliding of rock masses with maximal volume, which is usually considered in slope design.

It can be seen in table 2, that only 3 scars (on 25) have two lateral shear surfaces. That means that, for the other cases, the failure surface was visible at least on one side of the future scar. Table 2 also shows that only 3 failures affected a regular cliff surface (in horizontal and vertical cross-section).

Our results conduct us to propose that the detection of the prospective rock falls in the calcareous cliffs of the Subalpine Ranges should be based on the observation of the cliffs to look for the typical failure configurations that have been identified above. As direct observation from the marly slopes underlying the cliffs is not convenient (difficult access, low-angle view, visibility limited by forest), the proposed investigation method is the stereoscopic observation of aerial photographs taken from a helicopter.

Once a potentially unstable rock mass has been detected, its failure probability must be evaluated (usually for a period of the order of one century). The rock fall probability for different size rock falls can be evaluated for a general region where rock falls can occur in different specific locations (e.g. Wieczorek et al., 1999 ; Dussauge-Peisser et al., 2002), but the failure probability in a specific location can

be estimated only in a qualitative way (Jaboyedoff et al., 1999; Mazzocola and Sciesa, 2000; Dussauge, 2002). Our observations have shown that the joints, which constitute the failure surfaces, are usually not continuous and the failure occurs when the rock bridges have reached a critical size. Then the failure probability of a potentially unstable mass mainly depends on the proportion of rock bridges in the potential failure surface. The evaluation of this proportion is very difficult. Geophysical methods are being tested and some positive results have been obtained (Dussauge-Peisser et al., 2003).

7. Conclusions

The following conclusions concerning the calcareous cliffs in the Subalpine Ranges can be drawn from our observations.
(a) The observation of 25 rock falls made it possible to identify typical failure configurations (figure 4), which must be looked for in rock fall hazard detection.
(b) In the A and B configurations, the mean cliff surface is defined by one (or two) of the main joint sets and rock falls are due to morphologic irregularities of the cliff surface (figure 9) or to the dispersion of the joints around their average plane. Most of the failure surfaces could be seen before the rock fall occurs.
(c) The recommended investigation method for the detection of prospective rock falls consists in observing aerial photographs.
(d) The rock falls have been initiated by intact rock failure in rock bridges. Thus, the persistence of the joints appears to be the main factor to consider in the evaluation of the failure probability. Mechanical back analysis of the observed rock falls will be described in a further paper.
(e) Freeze-thaw cycles represent the main triggering factor of the observed rock falls. This suggests that ice jacking could cause microcrack propagation leading to failure. A slight influence of rainfall has been observed and no direct influence of earthquakes.

References

Aleotti, P., Chowdhury, R., 1999. Landslide hazard assessment: summary review and new perspectives, Bull Eng Geol Env 58, 21-44.

Antoine, P., Cruden, D.M., 1984. The slide from Mt. Granier, Isère and Savoie, France, on November 24, 1248. In: Proceedings of Int. Symp. on Landslides, Toronto, pp. 475-481.

Chau, K.T., Wong, R.H.C., Liu, J., Lee, C.F., 2003. Rockfall Hazard Analysis for Hong Kong Based on Rockfall Inventory. Rock Mechanics and Rock. Engineering 36 (5), 383-408.

Cheeney, R.F., 1983. Statistical methods in geology for field and lab decisions. George Allen & Unwin, London. 169 pp.

Coe, J.A., Harp, E.L., Tarr, A.C., Michael, J.A., 2005. Rock Fall Hazard Assessment of Little Mill Campground, American Fork Canyon, Uinta National Forest, Utah: U.S. Geological Survey Open-File Report 2005-1229, http://pubs.usgs.gov/of/2005/1229/.

Cruden, D.M., Varnes, D., J., 1996. Landslide types and processes. In: Turner, A.K., Schuster, R.L. (Eds), Landslides : Investigation and Mitigation. Transportation Research Board Special Report 247, National Academy Press, Washington, DC, pp. 36-75.

Dussauge-Peisser, C., 2002. Evaluation de l'aléa éboulement rocheux. PhD Thesis, Université Joseph Fourier, Grenoble, France. 222 pp.

Dussauge-Peisser, C., Helmstetter, A., Grasso, J.R., Hantz, D., Desvarreux, P., Jeannin, M., Giraud, A., 2002. Probabilistic approach to rock fall hazard assessment: potential of historical data analysis. Natural Hazard and Earth System Sciences 2, 1-13.

Dussauge-Peisser, C., Wathelet, M., Jongmans, D., Hantz, D., Couturier, B., Sintes, M., 2003. Investigation of a fractured limestone cliff (Chartreuse Massif, France) using seismic tomography and ground penetrating radar. *Near Surface Geophysics,* 2003, 161-170.

Eberhardt E., Stead D., Coggan J.S., 2004. Numerical analysis of initiation and progressive failure in natural rock slopes – the 1991 Randa rockslide. Int.J.Rock Mech. Min. Sci. 41, 69-87.

Einstein H.H., Veneziano D., Baecher G.B., OReilly K.J., 1983. The effect of discontinuity persistence on rock slope stability. Int.J.Rock Mech. Min. Sci. Geomech Abstr, 20(5), 227-236.

Evans, S.G., and Hungr, O., 1993. The assessment of rockfall hazard at the base of talus slopes: Canadian Geotechnical Journal, v. 30, p. 620–636.

Federico, A., Popescu, M., Fidelibus, C., Interno, G., 2004. On the prediction of the time of occurrence of a slope failure: a review. Landslides: Evaluation and Stabilization, Lacerda, Ehrlich, Fontoura & Sayao (eds), Taylor and Francis Group, London.

Frayssines, M., 2005. Contribution à l'évaluation de l'aléa éboulement rocheux. PhD thesis, Grenoble University.

Goodman, R.E., Shi, G.H., 1985. Block Theory and its Application to Rock Engineering. Prentice-Hall, London. 338 pp.

Guoguel, J., Pachoud, A., 1972. Géologie et dynamique de l'écroulement du Mont Granier. Bull. du BRGM, section 3, 1972 (1), 29-38.

Guzzetti, F., Carrara, A., Cardinali, M. and Reichenbach, P., 1999. Landslides hazard evaluation: a review of current techniques and their application in a multi-scale study, Central Italy. Geomorphology, 31: 181-216.

Guzzetti, F., Crosta, G., Detti, R., and Agliardi, F., 2002. STONE: a computer program for the three dimensional simulation of rock falls: Computers and Geosciences, v. 28, no. 9, p. 1,079–1,093.

Hantz, D., Vengeon, J.M., Dussauge Peisser C., 2003. An historical, geomechical and probabilistic approach to rock fall hazard assessment. Natural Hazard and Earth System Sciences 3, pp. 693-701.

Hatzfeld, D., RAP Working Group, 2003. Le Réseau Accélérométrique Permanent. Géologues, 135, pp. 31-35.

Hoek, E., Bray, J.W., 1981. Rock slope Engineering. The Institution of Mining and Metallurgy, London. 525 pp.

Hutchinson, J.N., 1988. General report : morphological and geotechnical parameters of landslides in relation to geology and hydrogeology. In: Bonnard, C. (Eds.), Proceedings of 5th International Symposium on Landslides, Lausanne, Switzerland, vol. 1, A.A. Balkema, Rotterdam, pp. 3-35.

IAEG Commission on Landslides, 1990. Suggested nomenclature for landslides. Bulletin of the International Association of Engineering Geology, 41, 13-16.

Jaboyedoff, M., Dudt, J.P., Labiouse, V., 2005. An attempt to refine rockfall hazard zoning based on the kinetic energy, frequency and fragmentation degree. Natural Hazards and Earth System Sciences, 5, 621-632.

Jaboyedoff, M., Baillifard, F., Marro, C., Philippossian, F., Rouiller, J.D., 1999. Detection of rock instabilities : Matterock methodology. In : Proceedings of the Joint Japan-Swiss Scientific Seminar on Impact Load by Rock falls and Design of Protection Structures, Kanazawa, pp. 37-43.

Jimenez, M. J., Giardini, D., Grünthal, G., SESAME Working Group, 2001. Unified seismic hazard modelling throughout the Mediterranean region. Bollettino di Geofisica Teorica ed Applicata, 42 (1-2), 3-18.

Keefer, D. K., 1984. Landslides caused by earthquakes. Geol. Soc. of A. Bull, 95 (4), 406-421.

Labiouse, V., 2004. Fragmental rockfall paths: comparison of simulations on Alpine sites and experimental investigation of boulder impacts. In Lacerda, Ehrlich, Fontoura and Sayao (Eds.), Landslides Evaluation and Stabilization, vol.1, Taylor and Francis Group, London, pp. 457-466.

Matsuoka, N., Sakai, H., 1999. Rockfall activity from an alpine cliff during thawing periods. Geomorphology 28: 309-328.

Mazzoccola, D., Sciesa, E., 2000. Implementation and comparison of different methods for rockfall hazard assessment in the Italian Alps. In: proceedings of 8th Int. Symp. on Landslides. Cardiff, Thomas Telford , pp. 1035-1040.

Robertson, A.M., 1970. The interpretation of geological factors for use in slope theory. In: Planning Open Pit Mines, Proceedings, Johannesburg, p. 55–71.

Rovera, G., 1990. Géomorphologie dynamique et aménagement des versants en Moyenne Tarentaise. PhD Thesis, Université Joseph Fourier, Grenoble, France. 465 pp.

Sandersen F., Bakkehøi S., Lied K., 1996. The influence of meteorological factors on the initiation of debris flows, rockfalls, rockslides and rockmass stability. In Senneset (Ed.): Landslides. Balkema, Rotterdam, 97-114.

Scavia, C., Barla, G., Bernaudo, V., 1990. Probabilistic stability analysis of block toppling failure in rock slope. Int. J. Rock Mech. Min. Sci. 27 (6), 465-478.

Serratrice J.F., Durville J.L., 1997. Description des roches et des massifs rocheux, exploitation de deux bases de données. Bulletin des Laboratoire des Ponts et Chaussées, 211, 73-87.

Terzaghi K., 1962. Stability of steep slopes on hard unweathered rock. Geotechnique 12, 251-270.

Thouvenot, F., Fréchet, J., 2004. Seismicity along the north-western edge of the Adria microplate. In: Pinter, N., Stein, S., Weber, J. (Eds.), The Adria Microplate. Kluwer, in press.

Varnes, D.J., Int. Association of Engineering Geology Commission on Landslides, 1984. Landslide hazard zonation : a review of principles and practice. In: Natural Hazards 3. UNESCO, Paris. 63 pp.

Wieczorek, G.F., Morrissey, M.M., Iovine, G., and Godt, J., 1999. Rock-fall potential in the Yosemite Valley, California: U.S. Geological Survey Open File Report 99-578, 1 plate 1:12.000, 7 p. http://greenwood.cr.usgs.gov/pub/open-file-reports/ofr-99-0578/

Wieczorek, G.F., and Snyder, J.B., 2004. Historical rock falls in Yosemite National Park:
U.S. Geological Survey Open-File Report 03-491. (http://pubs.usgs.gov/of/2003/of03-491/).
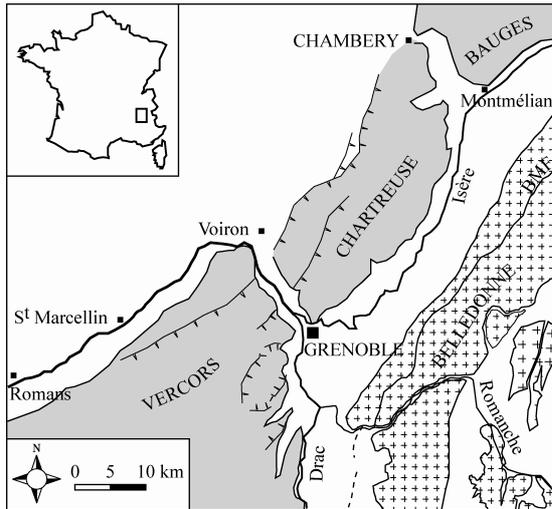
Fig. 1. Simplified tectonic map of the study area, with the sedimentary massifs (shaded), the external crystalline massifs (cross pattern) and the Belledonne Middle Fault (BMF).
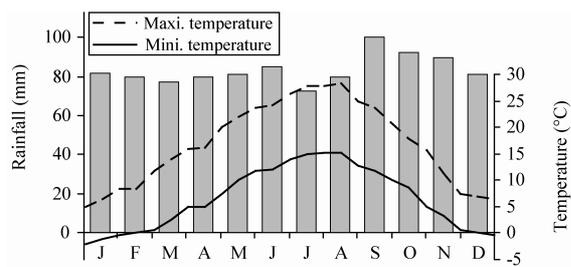

Fig. 2. Mean rainfall and temperature at Saint-Martin d'Hères station for the 1971-2000 period.
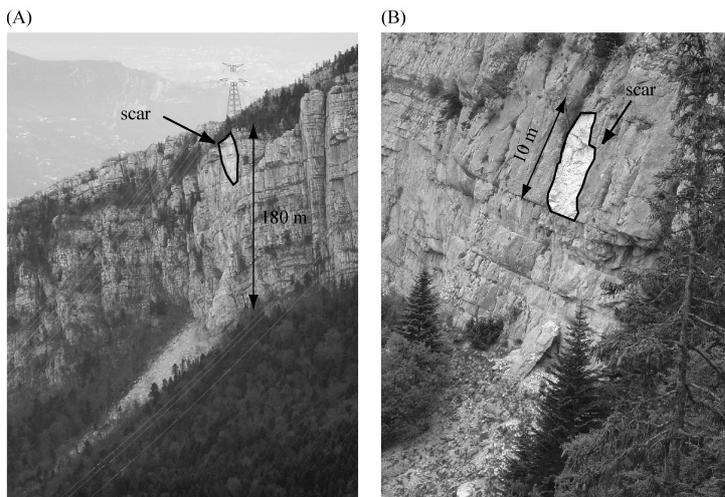

Fig. 3. (A) Dent du Loup rock fall and (B) Pas du Fouillet rock fall.

15
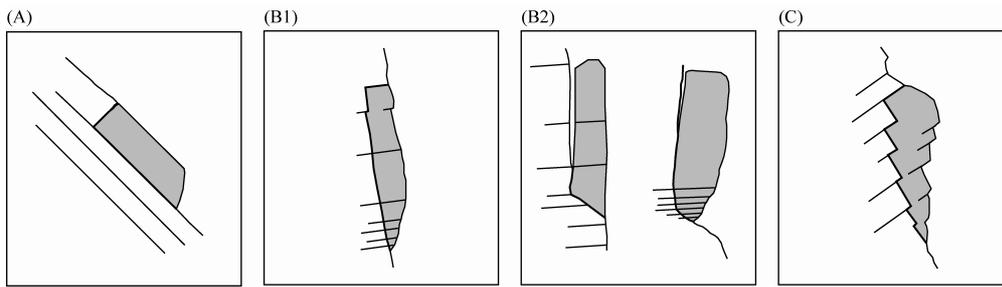
Fig. 4. Typical failure configurations. (A) Bedding conform to the slope, (B) bedding dipping less than 30° and joints defining a translational sliding (B1) or a composite sliding surface (B2), (C) bedding dipping more than 30° opposite to the slope.
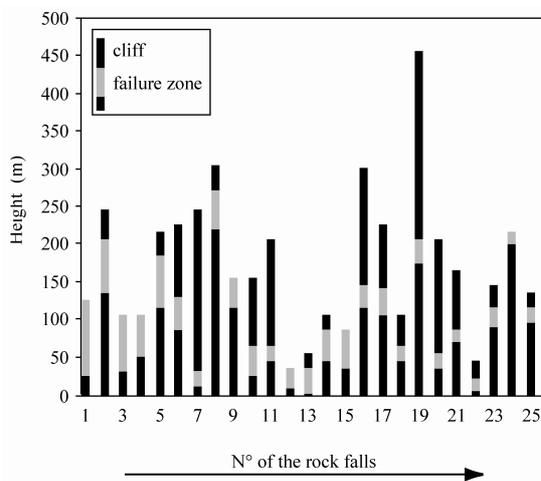


Fig. 5. Position of the scars on the cliff.
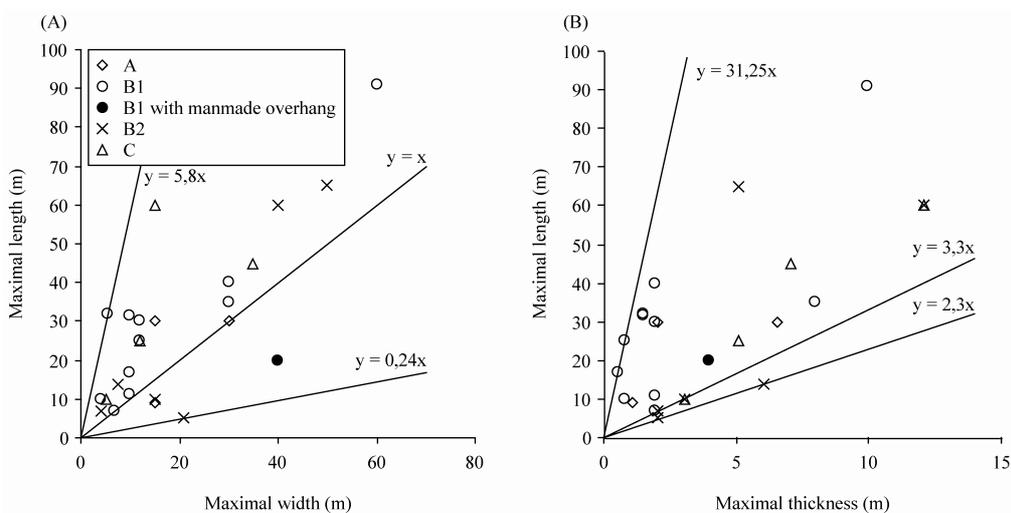
Fig. 6. Relation between the length and the width (A) and the length and the thickness (B) of the rock falls.
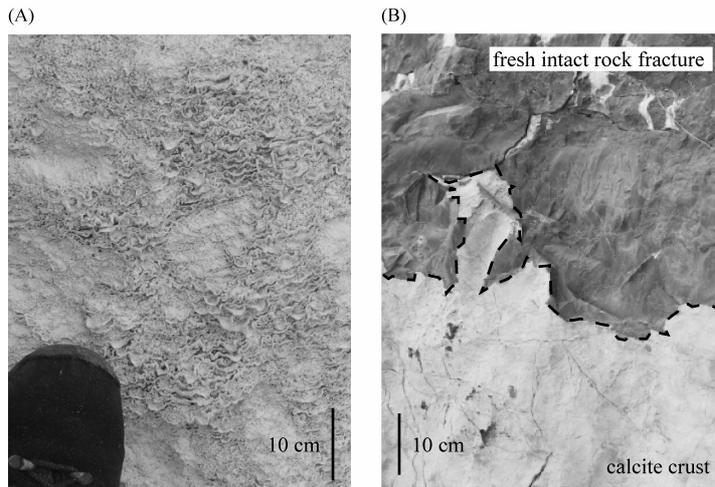
Fig. 7. Photographies of calcite concretions on Urgonian limestone (A) and fresh fracture surface in Tithonian limestone (B).

$$y = 0,1523x$$
$$R^2 = 0.748$$
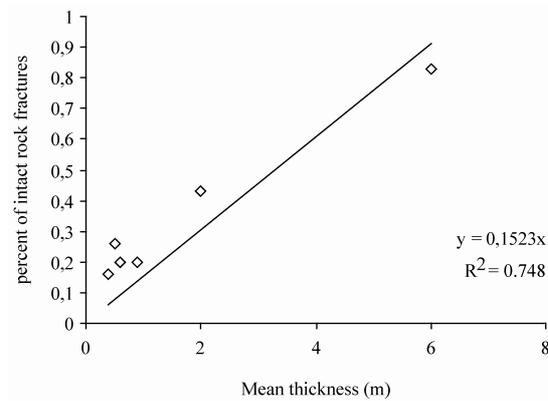
Fig. 8. Percentage of rock bridge versus mean thickness of slides.
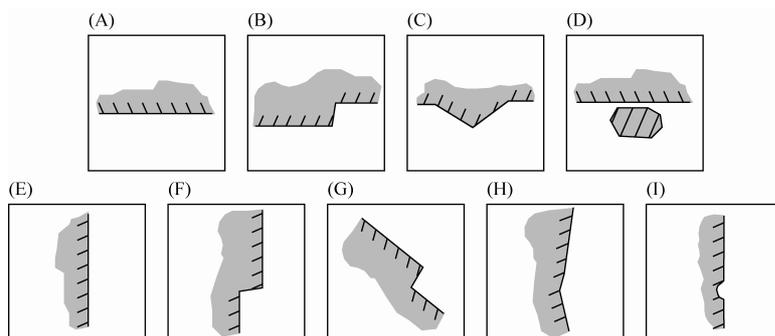
Fig. 9. Initial morphology of the fallen rock mass in a horizontal section (A to D) and in a vertical section (E to I). A : regular, B : step, C : spur, D : tower, E : regular, F : roof, G : inclined step, H : slightly overhanging, I : local overhang.
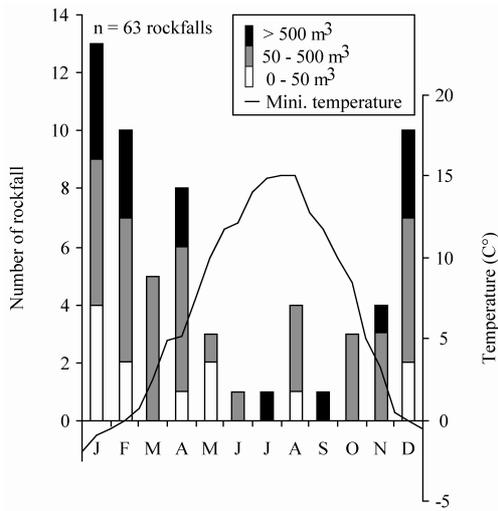
Fig. 10. Distribution of rock falls throughout the year for the 1948-2004 period and mean minimal temperature for the 1971-2000 period at Saint-Martin d'Hères station.
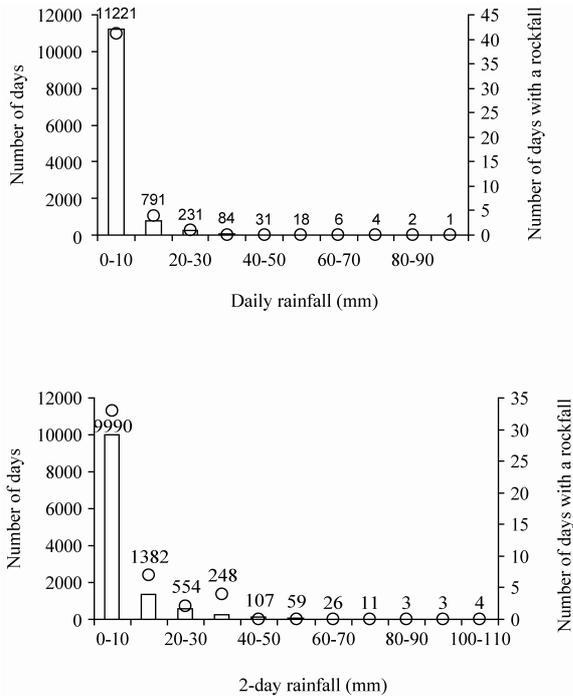
Fig. 11. (A) Distribution of the daily rainfall for the whole period (left, histogram) and for the days with a rock fall (right, circle), (B) distribution of the 2-day rainfall (rainfall of the day plus rainfall of the day before).
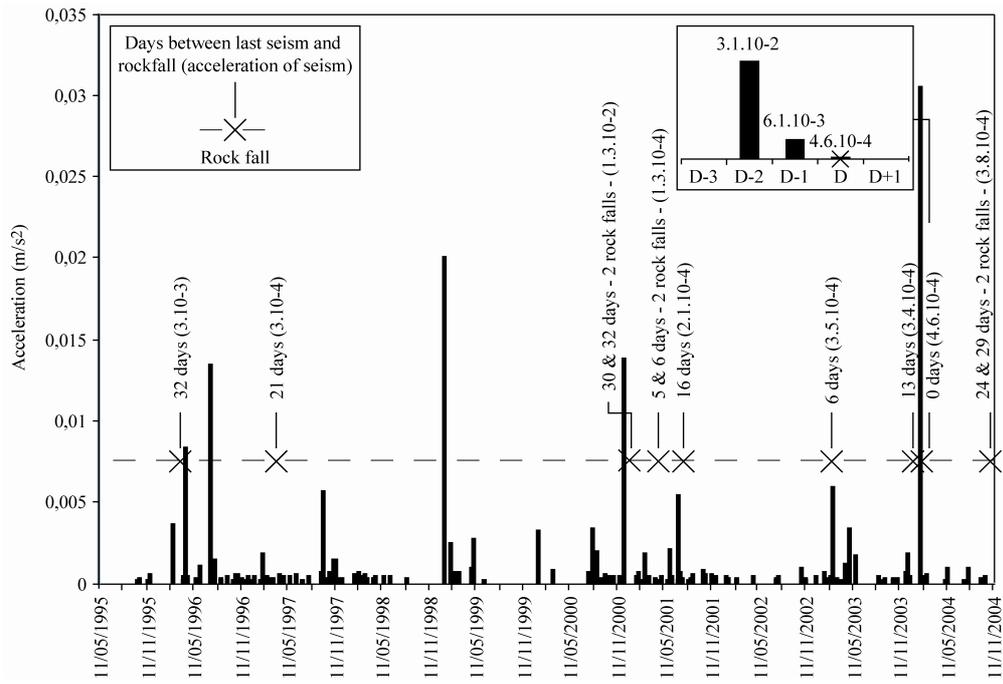
Fig. 12. Distribution of peak ground acceleration and rock falls from 11/05/1995 to 11/11/2004.
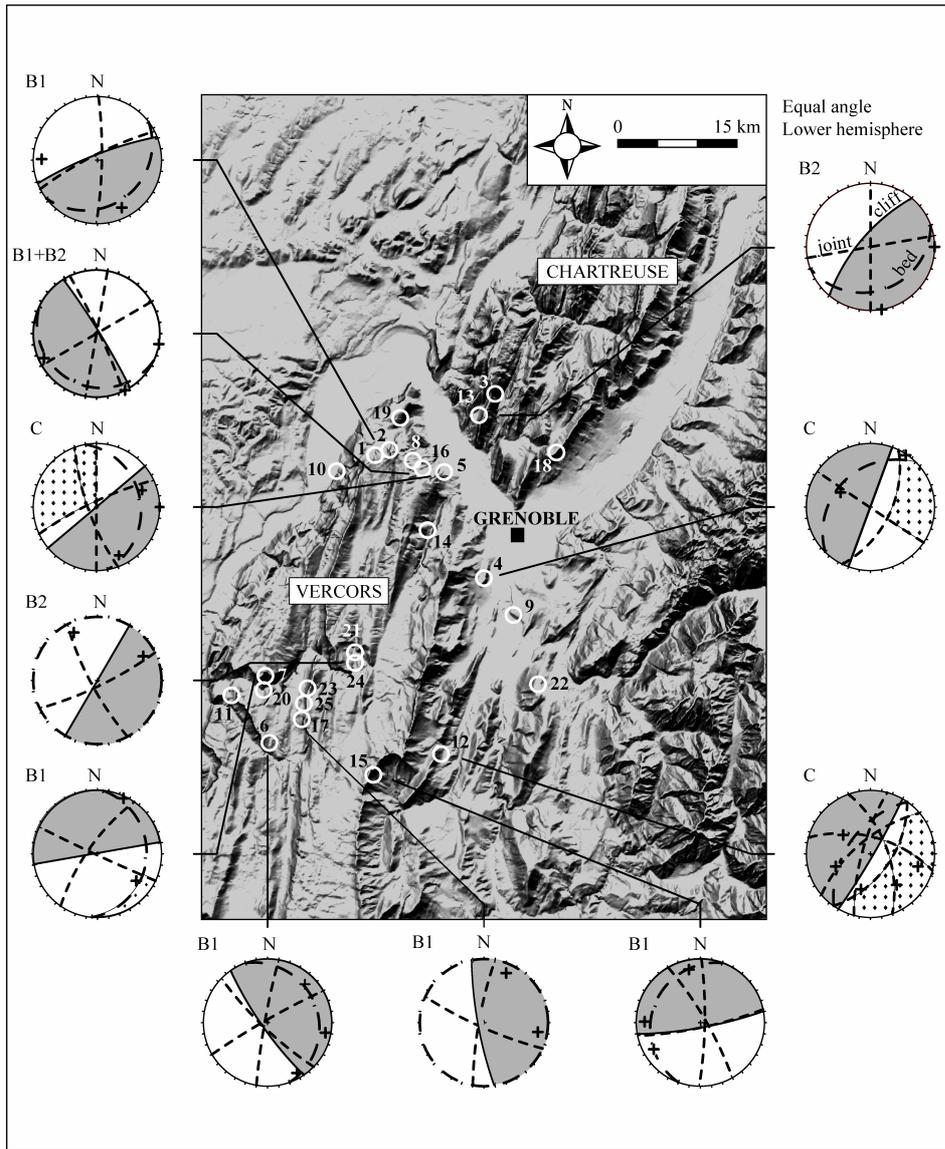
Fig. 13. Stereoplot of the mean joint planes (short dashed line), bedding plane (long dashed line) and mean cliff plane (continuous line) for different cliffs where rock falls occurred. Excavation pyramid (grey), critical joint pyramid (dotted surface), case number and configurations are notified.

Table 1
Chronological, geological and geometric data on rock falls.

| N°	Name	Date	Stage	Bedding		Maximal length (m)	Maximal width (m)	Area (m²)	Maximal thickness (m)	Mean thickness (m)	Volume (m³)
				/ Cliff	Dip (°)						
1	Combe Noire	30/01/1971	Urgonian	I	18	92	60	4,000	10	7.5	30,000
2	La Palette	20/04/1992	Urgonian	T	10-30	60	40	2,400	12	12	20,000
3	Chalais	22/03/1996	Valanginian	I	28	65	50	2,000	5	2.5	5,000
4	Comboire	06/02/1995	Tithonian	I	50	45	35	1,120	7	4	4,230
5	Dent du Loup	0h30 04/01/2001	Urgonian	I	30	60	15	550	12	6	3,500
6	Grands Goulets	14h31 21/02/2003	Urgonian	I	13	35	30	910	8	4	3,500
7	Ranc	18h00 30/01/2004	Urgonian	T	15-20	20	40	550	4	4.5	2,000
8	Echarina 1	~ 2000	Urgonian	I	10	40	30	1,015	2	1.5	1,500
9	Grand Rochefort	13/12/1990	Tithonian	C	80	30	30	500	2	2	900
10	Le Lignet	24/07/2001	Urgonian	C	46	30	15	340	6.5	4	660
11	La Charmate	20-21/04/2001	Urgonian	I	10	10	30	300	3	2	600
12	Eglise St Michel	31/03/1997	Tithonian	I	50	25	12	300	5	2	500
13	Cuchet	~ 2000	Valanginian	T	20	32	5.5	165	1.5	1.5	250
14	Furon	1999	Senonian	H	<10	30	12	360	2	0.7	250
15	Pas de la Balme	~ 2000	Urgonian	T	15	31.5	10	252	1.5	0.9	230
16	Echarina 2	09/2000 - 05/2002	Urgonian	I	10	10	7.5	75	6	2.5	150
17	Vierge du Vercors	11/2002	Urgonian	H	<10	25	12	235	0.8	0.5	117
18	Pas Guiguet	09/2000 - 10/2003	Tithonian	H	<10	11	10	110	2	1	110
19	Le Petit Chatelard	02/12/1992	Urgonian	C	45	9	15	135	1	0.7	100
20	Regard	?	Urgonian	?	?	7	7	50	2	2	100
21	Les Olivets	~ 2000	Urgonian	H	<10	5	21	70	2	2	90
22	Laffrey	02/01/2004	Lias	I	50	10	5	30	3	2	60
23	Chalimont	07/1998	Urgonian	H	<10	17	10	121	0.6	0.4	48
24	Goule Blanche	~ 2000	Urgonian	H	<10	7	4	28	2	1	30
25	Pas du Fouillet	~ 2000	Urgonian	H	<10	10	4	40	0.8	0.6	24

Table 2
Mechanical and morphological characteristics of rock falls.

N°	Name	Configuration	Failure mechanism	Dip of translational slide (°)	Lateral limits		Rear opening plane	Intact rock fracture		Calcite crust or concretion	Morphology before failure	
					Right	Left		Proportion (%)	Fracture mode			
1	Combe Noire	B1	planar slide	80	free	shear	no	?	-	?	regular	slightly overhanging
2	La Palette	B2	compound slide	45	free	shear	no	?	-	?	regular	regular
3	Chalais	B2	compound slide	70	free	free	no	?	-	?	spur	regular
4	Comboire	C	stepped slide	50	free	free	no	> 0.2	tensile	?	spur	inclined step
5	Dent du Loup	C	stepped slide	75-80	shear	shear	no	0.8	shear	yes	regular	regular
6	Grands Goulets	B1	planar slide	80-85	free	free	yes	2.5	?	yes	spur	roof
7	Ranc	B1	planar slide	85	shear	free	yes	5.0	?	yes	regular	roof
8	Echarina 1	B1	planar slide	85	shear	free	yes	?	-	?	regular	local overhang
9	Grand Rochefort	A	bed slide	60	shear	free	no	?	-	?	regular	inclined step
10	Le Lignet	A	bed slide	45	free	shear	yes	?	-	no	stepped	inclined step
11	La Charmate	B2	topple	-	free	shear	yes	?	-	?	regular	roof
12	Eglise St Michel	C	wedge slide	80	-	-	yes	0.4	?	yes	spur	?
13	Cuchet	B1	planar slide	70	free	free	yes	?	-	yes	spur	regular
14	Furon	B1	planar slide		free	free	yes	?	-	yes	spur	slightly overhanging
15	Pas de la Balme	B1	planar slide	75-80	free	free	no	0.2	shear	yes	spur	regular
16	Echarina 2	B2	wedge topple	-	-	-	yes	0.9	tensile	yes	spur	local overhang
17	Vierge du Vercors	B1	stepped planar slide	75-85	shear	free	no	0.3	shear	yes	regular	slightly overhanging
18	Pas Guiguet	B1	planar slide	-	free	free	yes	?	-	?	spur	slightly overhanging
19	Le Petit Chatelard	A	bed slide	45	shear	shear	yes	?	-	?	regular	inclined step
20	Regard	B1	planar slide	-	free	free	yes	?	-	?	spur	inclined step
21	Les Olivets	B2	planar slide	55	shear	shear	yes	0.6	shear	yes	regular	regular
22	Laffrey	C	stepped slide	65-75	free	shear	yes	?	-	?	spur	inclined step
23	Chalimont	B1	planar slide	85	shear	free	no	0.2	shear	yes	regular	regular
24	Goule Blanche	B2	wedge topple	-	-	-	yes	0.8	tensile	yes	spur	local overhang
25	Pas du Fouillet	B1	planar slide	85	free	shear	yes	0.2	shear	yes	regular	slightly overhanging

Table 3
Contingency table showing the relation between rock falls and the freeze-thaw cycles
(A) and seisms (B).

(A)

	Rockfall	No rockfall	Total
Freeze-thaw cycle	23	164,829	164,852
No freeze-thaw cycle	23	403,593	403,616
Total	46	568,422	568,468

(B)

	Rockfall	No rockfall	Total
1 seism	1	178	179
0 seism	11	2,603	2,614
Total	12	2,781	2,793